Preprints.org

Article

Not peer-reviewed version

Withdrawn: Rotating Black Holes: Continuum Failure Surfaces in Kerr Geometry

Michael Aaron Cody *

Posted Date: 11 December 2025

Withdrawn Date: 3 August 2026

doi: 10.20944/preprints202512.1076.v1

Preprints.org is a free multidisciplinary platform providing preprint service that is dedicated to making early versions of research outputs permanently available and citable. Preprints posted at Preprints.org appear in Web of Science, Crossref, Google Scholar, Scilit, Europe PMC, OpenAlex.

Copyright: This open access article is published under a Creative Commons CC BY 4.0 license, which permit the free download, distribution, and reuse, provided that the author and preprint are cited in any reuse.

Preprints.org (www.preprints.org) | NOT PEER-REVIEWED | Posted: 11 December 2025 doi:10.20944/preprints202512.1076.v1

Disclaimer/Publisher's Note: The statements, opinions, and data contained in all publications are solely those of the individual author(s) and contributor(s) and not of MDPI and/or the editor(s). MDPI and/or the editor(s) disclaim responsibility for any injury to people or property resulting from any ideas, methods, instructions, or products referred to in the content.

Article

Withdrawn: Rotating Black Holes Continuum Failure Surfaces in Kerr Geometry

Michael Aaron Cody

Independent Researcher, USA; mac92Contact@gmail.com

Withdrawal Statement

This preprint was retracted at the authors' request due to serious scientific errors that cannot be corrected by updating the paper.

WITHDRAWAL

in closed form from standard geometric treatments [2]. The purpose of this paper is to compute $\sigma(r,\theta) = \sqrt{|K(r,\theta)|}$ for the Kerr spacetime, to impose the condition $\sigma(r,\theta) = \sigma_c$, and to solve for a latitude-dependent radius $r_c(\theta)$ that marks the boundary at which the continuum description fails.

© 2025 by the author(s). Distributed under a Creative Commons CC BY license.

Preprints.org (www.preprints.org) | NOT PEER-REVIEWED | Posted: 11 December 2025 doi:10.20944/preprints202512.1076.v1

The resulting surface is compared with the Schwarzschild value r_c, with the Kerr horizons $r_\pm$, and with the structure of the ring singularity at $r = 0$ on the equatorial plane. The analysis shows how rotation modifies the onset of continuum failure and clarifies the geometric structure expected inside rotating collapse.

2. Kerr Geometry Setup

The rotating vacuum solution of Einstein's field equations is described by the Kerr metric in Boyer-Lindquist coordinates (t, r, θ, ϕ), with mass parameter M and angular momentum per unit mass a. The metric takes the standard form

$$ds^2 = -\left(1 - \tfrac{2Mr}{\Sigma}\right)dt^2 - \tfrac{4Mar\sin^2\theta}{\Sigma}\,dt\,d\phi + \tfrac{\Sigma}{\Delta}\,dr^2 + \Sigma\,d\theta^2 + \left(r^2 + a^2 + \tfrac{2Ma^2 r\sin^2\theta}{\Sigma}\right)\sin^2\theta\,d\phi^2, \quad (1)$$

where the functions Δ and Σ are defined explicitly by

$$\Delta = r^2 - 2Mr + a^2, \quad (2)$$

$$\Sigma = r^2 + a^2\cos^2\theta. \quad (3)$$

The signature convention is $(-,+,+,+)$, and units are chosen such that $G = c = 1$. These quantities appear in all curvature components and determine the geometric structure of the spacetime. The coordinate domain is $r > 0$ and $0 \le \theta \le \pi$, with the azimuthal angle $0 \le \phi < 2\pi$ and unrestricted time coordinate t. The invariance of the geometry under the reflection $\theta \mapsto \pi - \theta$ reduces the physically distinct domain to $0 \le \theta \le \pi/2$ for the curvature analysis that follows. This reduction applies specifically to scalar invariants such as the Kretschmann scalar, since these quantities depend on $\cos\theta$ and therefore remain unchanged under $\theta \to \pi - \theta$. The full metric is defined on the entire interval $0 \le \theta \le \pi$, but no loss of generality occurs when restricting scalar curvature computations to the half-interval.

Several geometric structures play a central role in Kerr spacetime. The roots of Δ determine the horizon radii

$$r_\pm = M \pm \sqrt{M^2 - a^2}, \quad (4)$$

which exist only when $|a| \le M$. The outer value r_+ is the event horizon and the inner value r_- is the Cauchy horizon. Both positions correspond to coordinate singularities rather than curvature singularities, and they are identified through the vanishing of Δ rather than the vanishing of Σ. The ergosurface is defined by the condition $g_{tt} = 0$, which occurs when $1 - 2Mr/\Sigma = 0$. Because Σ depends on θ, the ergosurface is not spherical but bulges outward near the equatorial region. The ergoregion is the domain in which the Killing vector ∂_t becomes spacelike, and its boundary depends smoothly on θ. This structure is distinct from the event horizon and will not play a direct role in the failure condition, but its geometry reinforces the fact that rotation introduces anisotropy into all curvature quantities. The curvature singularity of the Kerr solution is not pointlike. At $r = 0$, the quantity Σ reduces to $a^2\cos^2\theta$, which vanishes only when $\theta = \pi/2$. This produces the ring singularity familiar from standard treatments of Kerr geometry. Along the rotation axis, where $\theta = 0$ or $\theta = \pi$, the expression $\Sigma = r^2 + a^2\cos^2\theta$ remains nonzero for all $r > 0$, and the metric components remain finite except at the horizon positions. This property will be relevant when evaluating the curvature invariant, since the vanishing of Σ governs the divergence structure of the Kretschmann scalar. In particular, the fact that Σ does not vanish on the axis ensures that the stress invariant $\sigma = \sqrt{|K|}$ remains finite at $r = 0$ along the axis, whereas it diverges on the equatorial ring. This axial regularity is a geometric feature unique to rotating solutions and distinguishes the Kerr interior structure from the Schwarzschild case.

3. Kerr Kretschmann Scalar $K(r, \theta)$

The Kretschmann scalar $K(r, \theta)$ encodes the local curvature strength of the Kerr spacetime. The expression is algebraically nontrivial but can be factored into explicit polynomial components. The

WITHDRAWAL

© 2025 by the author(s). Distributed under a Creative Commons CC BY license.

Preprints.org (www.preprints.org) | NOT PEER-REVIEWED | Posted: 11 December 2025 doi:10.20944/preprints202512.1076.v1

scalar is analyzed here in its canonical form, followed by expansion of numerator polynomials, limiting case evaluations, and sign-structure implications.

Canonical form. The expression for the Kretschmann scalar in Kerr geometry is given by Henry (2000) [3] as

$$K = \frac{48M^2\left(r^2 - a^2\cos^2\theta\right)\left[\left(r^2 - a^2\cos^2\theta\right)^2 - 16r^2a^2\cos^2\theta\right]}{\Sigma^6}, \tag{5}$$

with $\Sigma = r^2 + a^2\cos^2\theta$. Notation follows Carroll (2004) [4] and Poisson (2004) [5].

Polynomial expansion. The squared term expands directly:

$$\left(r^2 - a^2\cos^2\theta\right)^2 = r^4 - 2a^2r^2\cos^2\theta + a^4\cos^4\theta.$$

Substituting into the bracket yields

$$r^4 - 2a^2r^2\cos^2\theta + a^4\cos^4\theta - 16r^2a^2\cos^2\theta = r^4 - 18a^2r^2\cos^2\theta + a^4\cos^4\theta.$$

The numerator becomes

$$N(r,\theta) = 48M^2\left(r^2 - a^2\cos^2\theta\right)\left(r^4 - 18a^2r^2\cos^2\theta + a^4\cos^4\theta\right). \tag{6}$$

The denominator Σ^6 remains factored for singularity structure analysis.

Limiting cases. The following limiting behaviors verify the expression's physical consistency:

- *Schwarzschild limit* ($a \to 0$):
$$K \to \frac{48M^2r^2 \cdot r^4}{r^{12}} = \frac{48M^2}{r^6},$$
matching the Schwarzschild scalar curvature [6].
- *Equatorial plane* ($\theta = \frac{\pi}{2}$): At $\cos\theta = 0$,
$$K = \frac{48M^2r^2 \cdot r^4}{(r^2)^6} = \frac{48M^2}{r^6},$$
recovering the Schwarzschild form since the equatorial plane exhibits no frame-dragging contribution to radial curvature.
- *Polar axis* ($\theta = 0$): At $\cos\theta = 1$, $\Sigma = r^2 + a^2 > 0$, and the numerator remains finite:
$$K \sim \frac{\text{finite}}{(r^2 + a^2)^6}.$$
- *Ring singularity* ($\Sigma \to 0$): At $r = 0$, $\theta = \frac{\pi}{2}$, the function $\Sigma = 0$, and
$$K \to \infty,$$
confirming scalar curvature divergence at the ring singularity [2].

Sign-change surfaces. The Kretschmann scalar is not sign-definite in Lorentzian signature. The numerator vanishes when either of the following conditions is met:

$$\text{Zero Set 1:} \quad r^2 - a^2\cos^2\theta = 0,$$

$$\text{Zero Set 2:} \quad r^4 - 18a^2r^2\cos^2\theta + a^4\cos^4\theta = 0.$$

These surfaces define transitions between $K > 0$ and $K < 0$ regions. The sign structure follows directly from the factorized form of the numerator [7].

WITHDRAWAL

© 2025 by the author(s). Distributed under a Creative Commons CC BY license.

Preprints.org (www.preprints.org) | NOT PEER-REVIEWED | Posted: 11 December 2025 doi:10.20944/preprints202512.1076.v1

Physical implications. Negative values of K require using the modulus:

$$\sigma = \sqrt{|K|}.$$

Numerical schemes must detect and track zero-crossings of K to ensure proper root-finding for curvature divergence thresholds and failure conditions.

4. Substrate Stress Field $\sigma(r, \theta)$

The stress field $\sigma(r, \theta)$ is defined as the local curvature magnitude extracted from the Kretschmann scalar. It acts as a diagnostic for continuum-level failure in the relativistic substrate model and encodes directional dependence from the Kerr geometry.

Definition. The field is defined pointwise in terms of the Kretschmann scalar:

$$\sigma(r, \theta) = \sqrt{|K(r, \theta)|}.$$

This expression ensures that σ remains real-valued even when K is negative, as occurs in certain angular regions of Kerr spacetime [7].

Interpretation. The function $\sigma(r, \theta)$ encodes the intrinsic curvature stress induced by the gravitational field. The quantity has units of inverse length squared:

$$[K] = L^{-4} \quad \Rightarrow \quad [\sigma] = \sqrt{L^{-4}} = L^{-2}.$$

A critical stress threshold $\sigma = \sigma_c$ is used to indicate continuum failure, consistent with substrate stress models [1,8].

Contrast with Schwarzschild. In the Schwarzschild solution, the Kretschmann scalar depends only on the radial coordinate, yielding

$$K_{\text{Sch}}(r) = \frac{48M^2}{r^6} \quad \Rightarrow \quad \sigma(r) = \sqrt{\frac{48M^2}{r^6}} = \frac{\sqrt{48}M}{r^3}.$$

This function is monotonic in r, and the condition $\sigma = \sigma_c$ yields a unique failure radius r_c. In contrast, the Kerr geometry produces an angularly anisotropic curvature field $\sigma(r, \theta)$, and the failure condition $\sigma = \sigma_c$ defines a surface in spacetime rather than a single radial value. Anisotropy is a direct result of spin-coupled curvature distortion [2].

Behavior near special directions. The stress field exhibits qualitatively distinct behavior along principal directions of the geometry:

- *Equator* ($\theta = \frac{\pi}{2}$): The function $\sigma(r, \theta)$ diverges as $r \to 0$ due to the ring singularity. This direction corresponds to maximal stress concentration.
- *Axis* ($\theta = 0$): The value of $\sigma(r, \theta)$ remains finite even at $r = 0$. From Section 3, the explicit expression at the origin on the axis is

$$\sigma(0, 0) = \sqrt{\left| -\frac{48M^2}{a^6} \right|} = \frac{\sqrt{48}\, M}{a^3},$$

corresponding to the minimal stress magnitude in the geometry. This is the corrected result discussed in the curvature analysis [3].

5. Failure Condition: $\sigma(r, \theta) = \sigma_c$

Failure is defined to occur when the local stress field exceeds a critical threshold:

$$\sigma(r, \theta) = \sigma_c.$$

WITHDRAWAL

© 2025 by the author(s). Distributed under a Creative Commons CC BY license.

Preprints.org (www.preprints.org) | NOT PEER-REVIEWED | Posted: 11 December 2025 doi:10.20944/preprints202512.1076.v1

This yields an equation that locates the failure surface implicitly in the Kerr spacetime.

Core equation. By squaring both sides, the failure condition becomes:

$$|K(r,\theta)| = \sigma_c^2.$$

This defines a hypersurface in the (r,θ) plane where curvature stress reaches the failure threshold.

Explicit substitution. Using the expanded expression for $K(r,\theta)$ from Section 3, the equation becomes:

$$\left| \frac{48M^2\left(r^2 - a^2\cos^2\theta\right)\left(r^4 - 18a^2r^2\cos^2\theta + a^4\cos^4\theta\right)}{\left(r^2 + a^2\cos^2\theta\right)^6} \right| = \sigma_c^2.$$

This step retains the full polynomial structure in both numerator and denominator. No compression or factor cancellation is applied, as the full functional form is required for numerical root detection.

The failure equation is a sixth-order rational expression in r, with angular dependence through $\cos^2\theta$ and $\cos^4\theta$. The absolute value introduces a piecewise structure based on the sign of the original curvature scalar. The equation is strongly nonlinear and cannot be solved analytically for $r(\theta)$. Numerical root-finding is therefore necessary at each value of θ. The equation is nonlinear in both numerator and denominator, and no algebraic inversion is available.

The equation is only evaluated within the physically meaningful region:

$$r > 0, \quad 0 \le \theta \le \frac{\pi}{2}$$

The lower hemisphere is excluded by symmetry. The singularity, where $\Sigma = r^2 + a^2\cos^2\theta = 0$, must be avoided, as the curvature diverges there and the equation becomes ill-defined. This expression for Σ was introduced in Section 3. The singularity occurs precisely at $r = 0$, $\theta = \frac{\pi}{2}$.

Root structure. Because the equation includes an absolute value, valid solutions for r may occur on either side of the zero sets of the Kretschmann scalar. From Section 3, these zero sets occur when:

$$r^2 - a^2\cos^2\theta = 0,$$

$$r^4 - 18a^2r^2\cos^2\theta + a^4\cos^4\theta = 0.$$

Numerical solvers must detect crossings of these surfaces to properly bracket roots. Root isolation requires careful domain scanning and piecewise evaluation to ensure that both positive and negative regions of K are included. The absolute value enforces continuity in σ, but the underlying rational function is sign-sensitive. Bracketing methods must be robust to this discontinuity in the sign of the numerator. In addition, regions near the singularity at $\Sigma \to 0$ may require exclusion or adaptive resolution to prevent divergence in numerical evaluation.

6. Numerical Reconstruction of Failure Surface $r_c(\theta)$

The critical radius function $r_c(\theta)$ defines the locus at which the local stress $\sigma(r,\theta)$ reaches the failure threshold σ_c. This section describes the reconstruction of this failure surface using direct numerical evaluation of the curvature field.

Precomputed subexpressions. The following auxiliary functions are defined to simplify repeated evaluation of the stress field:

$$L(r,\theta) = r^2 - a^2\cos^2\theta,$$

$$B(r,\theta) = r^4 - 18a^2r^2\cos^2\theta + a^4\cos^4\theta,$$

$$\Sigma(r,\theta) = r^2 + a^2\cos^2\theta.$$

WITHDRAWAL

© 2025 by the author(s). Distributed under a Creative Commons CC BY license.

Preprints.org (www.preprints.org) | NOT PEER-REVIEWED | Posted: 11 December 2025 doi:10.20944/preprints202512.1076.v1

The function Σ is strictly positive for all $r > 0$, $\theta \in [0, \pi/2)$, except at the singular ring $r = 0$, $\theta = \frac{\pi}{2}$, where it vanishes and the curvature diverges. The Kretschmann scalar and derived stress field are:

$$K(r,\theta) = \frac{48M^2 \cdot L(r,\theta) \cdot B(r,\theta)}{\Sigma(r,\theta)^6},$$

$$\sigma(r,\theta) = \sqrt{|K(r,\theta)|}.$$

Failure function. The failure condition is formulated as the root of the scalar function:

$$F(r,\theta) = |K(r,\theta)| - \sigma_c^2.$$

The critical radius $r_c(\theta)$ is defined implicitly as the solution to $F(r,\theta) = 0$ for fixed θ. This is equivalent to:

$$F(r,\theta) = 0 \quad \Leftrightarrow \quad \sigma(r,\theta) = \sigma_c.$$

Numerical method. The reconstruction proceeds as follows:

- Select a uniform angular grid $\{\theta_i\}$ in the range $[0, \frac{\pi}{2}]$.
- For each θ_i, define a radial search interval $r \in [r_{\min}, r_{\max}]$, where the lower bound excludes the singular ring ($r > 0$), and the upper bound extends beyond both Kerr horizons.
- Evaluate $F(r,\theta_i)$ at discretized points within this interval. Identify adjacent pairs (r_j, r_{j+1}) where F changes sign, indicating a root bracket. The function F is continuous in r across this domain (except at the singularity), and therefore standard bracketing methods such as bisection are applicable.
- Apply a root-finding method (e.g., bisection or Ridder's algorithm) to solve $F(r,\theta_i) = 0$ to desired precision.
- In cases where the sign change occurs near known curvature zero sets (Section 3), ensure numerical continuity across regions where the sign of $K(r,\theta)$ flips. Discontinuities in the numerator sign structure require robust bracketing.

The result is a discrete set of angular-radius pairs $(\theta_i, r_c(\theta_i))$ forming a sampled representation of the failure surface. This data can be used for both quantitative and geometric comparisons:

- A polar plot of $r = r_c(\theta)$ visualizes the anisotropic structure of the failure surface.
- The surface may be compared directly to the Kerr horizons:

$$r_\pm = M \pm \sqrt{M^2 - a^2}.$$

These are shown for reference only; the failure surface is determined independently by the curvature field and does not coincide with causal boundaries.

7. Geometry of the Failure Surface

The failure surface defined by $\sigma(r,\theta) = \sigma_c$ exhibits distinct geometric structure due to the anisotropic curvature distribution in Kerr spacetime. This section characterizes its shape, topology, and relation to known features of the Kerr geometry.

Overall topology. The surface $r = r_c(\theta)$ is rotationally symmetric about the spin axis of the black hole. It does not form a sphere unless the spin parameter vanishes ($a = 0$), in which case the spacetime reduces to Schwarzschild and the failure surface becomes a sphere of radius r_c. For all $a > 0$, the surface remains simply connected and continuous, not toroidal or self-intersecting. Its anisotropic geometry reflects the spin-induced curvature distortion described in [7,9].

WITHDRAWAL

© 2025 by the author(s). Distributed under a Creative Commons CC BY license.

Preprints.org (www.preprints.org) | NOT PEER-REVIEWED | Posted: 11 December 2025 doi:10.20944/preprints202512.1076.v1

Equatorial behavior. At the equator ($\theta = \pi/2$), the Kretschmann scalar diverges at the ring singularity ($r = 0$), and stress magnitudes are maximized. This results in the failure surface extending furthest outward near the equator:

$$r_c\left(\frac{\pi}{2}\right) = \max_\theta r_c(\theta).$$

This agrees with curvature-driven stress peaking along the plane of rotation, consistent with analyses of curvature invariants in spinning spacetimes [3,10].

Axial behavior. Along the polar axis ($\theta = 0$), the curvature scalar remains finite even as $r \to 0$, and the stress field $\sigma(r, 0)$ remains bounded. This causes the failure radius to be minimized along the spin axis:

$$r_c(0) = \min_\theta r_c(\theta).$$

This behavior contrasts with isotropic models and highlights the axis-protecting structure of Kerr curvature. A result consistent with differential behavior of scalar invariants noted in [8,10].

Shape characterization. The resulting failure surface is oblate: the radius at the equator exceeds that at the pole. Define the polar compression ratio:

$$f = \frac{r_c(\pi/2) - r_c(0)}{r_c(0)}.$$

This provides a coordinate-invariant measure of axial flattening due to spin-induced curvature distortion. Note that this differs from the standard geodetic flattening convention, which typically uses the equatorial radius in the denominator. The shape resembles that of isocurvature contours in Kerr-Newman geometry, though it is not directly tied to horizons or ergosurfaces [4,5].

Extremal limit behavior. As the spin approaches extremality ($a \to M$), the anisotropy of the curvature field increases significantly:

- The equatorial region experiences sharply increasing curvature, pushing the failure surface further outward.
- The axis remains regular and curvature-limited, preserving the protected behavior at $\theta = 0$.
- The failure surface may approach or intersect the outer horizon r_+, depending on the threshold σ_c. In extremal cases, partial overlap may occur.

These effects parallel the known amplification of frame-dragging and equatorial curvature in the extremal Kerr geometry [9,11].

Comparison with Kerr horizons. The reconstructed surface $r = r_c(\theta)$ can be compared against the Kerr horizons:

$$r_\pm = M \pm \sqrt{M^2 - a^2}.$$

Three distinct regimes are possible:

- $r_c(\theta) > r_+$: failure surface lies entirely outside the event horizon.
- $r_- < r_c(\theta) < r_+$: failure occurs inside the ergoregion but outside the Cauchy horizon.
- $r_c(\theta) < r_-$: failure occurs in a deeply sub-horizon region, not causally accessible from outside.

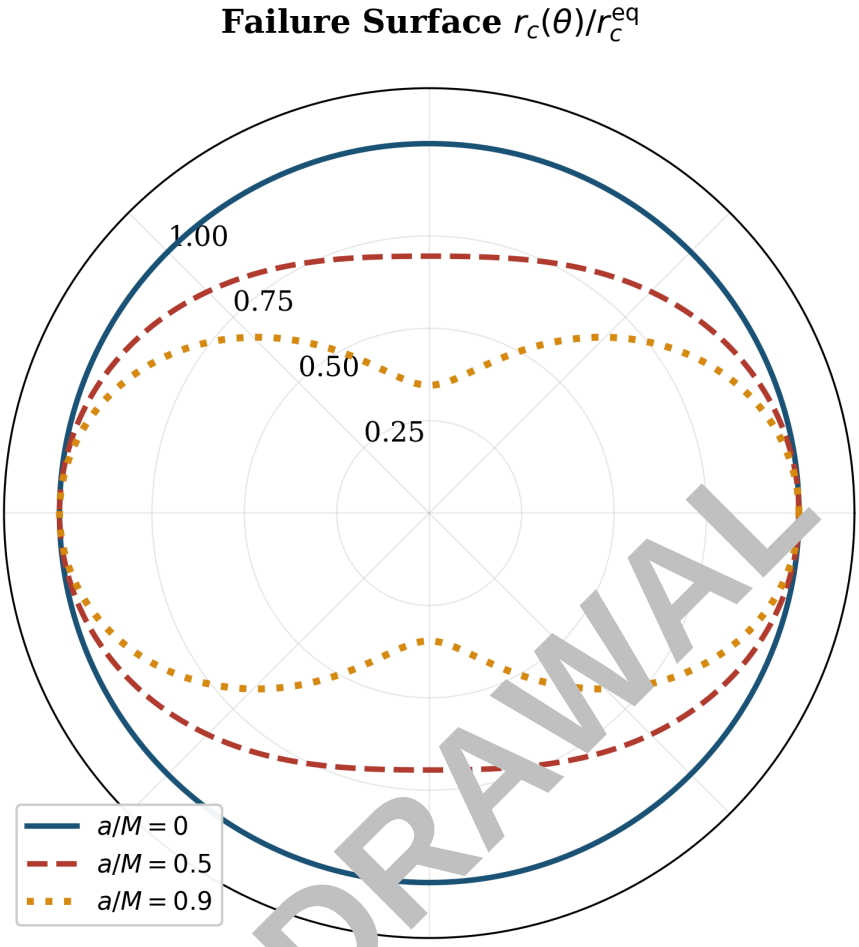
These comparisons provide geometric constraints on where the continuum description may break down and are consistent with the stress-based failure threshold model introduced earlier [1].

Taken together, these features establish that the condition $\sigma(r, \theta) = \sigma_c$ defines a smooth, closed surface whose shape is determined entirely by the anisotropic curvature distribution of the Kerr geometry. While the analytic expressions clarify how the stress field behaves along principal directions, the global structure of the failure surface is most transparently illustrated in a meridional cross–section. The figure below visualizes $r_c(\theta)$ for several spin parameters, emphasizing the transition from the spherical Schwarzschild case to the increasingly oblate geometry that emerges as the rotation approaches extremality.

WITHDRAWAL

© 2025 by the author(s). Distributed under a Creative Commons CC BY license.

Preprints.org (www.preprints.org) | NOT PEER-REVIEWED | Posted: 11 December 2025 doi:10.20944/preprints202512.1076.v1



WITHDRAWAL

Figure 1. *Meridional cross-section of the failure surface $r_c(\theta)$ for several Kerr spin parameters, normalized to the equatorial value. The Schwarzschild case ($a = 0$) reproduces a spherical boundary. Increasing spin introduces oblateness: the failure radius is largest at the equator and smallest along the rotation axis, reflecting the anisotropic curvature distribution of the Kerr geometry.*

8. Physical Interpretation

The existence of a stress-limited surface $r = r_c(\theta)$ implies that classical gravitational collapse in a rotating configuration may terminate at a finite, anisotropic boundary. Below this surface, the curvature stress exceeds the critical threshold σ_c, and the continuum description of the spacetime ceases to be valid. The internal geometry can no longer be described by the Kerr solution, and the evolution of the system may require a discrete or quantum extension of the underlying degrees of freedom [8,12]. The traditional Kerr ring singularity occurs at $\Sigma = 0$, corresponding to $r = 0, \theta = \pi/2$. In the presence of a finite failure threshold, the stress field $\sigma(r, \theta)$ diverges before this point is reached. As a result, no region of spacetime reaches $\Sigma = 0$, and the ring singularity is never physically realized. The failure surface thus functions as a natural regulator that prevents access to classically pathological zones, without invoking exotic energy conditions.

The rotation-induced curvature anisotropy causes collapse to terminate at different radii depending on direction. Near the equator, curvature invariants diverge more strongly, and the failure radius $r_c(\pi/2)$ is largest. Near the poles, curvature remains bounded and collapse proceeds deeper. This produces an oblate failure geometry, compressed along the spin axis and extended along the equatorial plane. This anisotropic internal structure is a direct consequence of the spin-coupled curvature distribution encoded in the Kerr geometry [2,9,10].

If the critical stress σ_c corresponds to a curvature scale attainable in realistic gravitational collapse, the presence of a finite failure surface may have observable consequences:

© 2025 by the author(s). Distributed under a Creative Commons CC BY license.

Preprints.org (www.preprints.org) | NOT PEER-REVIEWED | Posted: 11 December 2025 doi:10.20944/preprints202512.1076.v1

- The effective location of the innermost stable circular orbit (ISCO) may shift, potentially modifying ringdown signals from merging black holes [13].
- Jet-launching regions could be influenced by the altered geometry near the poles, where failure occurs closer to the rotation axis [14].
- The failure surface may produce boundary-like effects that alter matter or field propagation in the near-horizon regime.

These implications remain speculative and depend on the value of σ_c, which may be set by quantum gravity or sub-continuum physics. No definite astrophysical predictions are made here. Beyond these phenomenological considerations, several approaches in quantum gravity have proposed mechanisms to avoid singularities inside black holes. These include fuzzball geometries in string theory [15], gravastar models with phase transitions [16], and polymer quantization in loop quantum gravity [17]. The present model differs in that it does not introduce exotic matter, boundary matching, or fundamental discretization by hand. Instead, singularity avoidance emerges from a classical geometric failure condition defined within the continuum itself, rooted in the divergence of the curvature stress field.

9. Towards Deriving the Stress Threshold σ_c

The curvature stress threshold σ_c introduced in this framework defines the limit beyond which the continuum description of spacetime ceases to be valid. While this paper treats σ_c as a phenomenological parameter, it is natural to ask whether its value can be estimated or motivated from quantum gravitational considerations. This section outlines candidate approaches that may constrain or motivate σ_c based on known quantum geometry models.

One natural assumption is that the breakdown of the continuum occurs when curvature invariants reach the Planck scale. The Kretschmann scalar K has units of inverse length to the fourth power, i.e.,

$$[K] = \left[L^{-4}\right],$$

which implies that $\sigma(r,\theta) = \sqrt{|K|}$ has units

$$[\sigma] = \left[L^{-2}\right].$$

By dimensional analysis, a natural quantum gravity curvature scale is set by the Planck length:

$$\ell_{\mathrm{P}} = \sqrt{\frac{\hbar G}{c^3}}.$$

The associated Planck-scale stress threshold is then:

$$\sigma_c^{(\mathrm{Planck})} = \frac{1}{\ell_{\mathrm{P}}^2}.$$

This provides a baseline estimate. The corresponding Kretschmann scalar at failure would be:

$$K_c = \sigma_c^2 = \frac{1}{\ell_{\mathrm{P}}^4}.$$

This value is not derived from any specific quantum gravity model, but it is consistent with upper bounds on curvature inferred in polymer quantized spacetimes [17,18].

An alternative motivation comes from entropy density. The Bekenstein-Hawking entropy for a black hole is:

$$S = \frac{k_B A}{4\ell_{\mathrm{P}}^2},$$

WITHDRAWAL

© 2025 by the author(s). Distributed under a Creative Commons CC BY license.

Preprints.org (www.preprints.org) | NOT PEER-REVIEWED | Posted: 11 December 2025 doi:10.20944/preprints202512.1076.v1

and the area A scales with r^2. A local entropy density ρ_S then scales as:

$$\rho_S \sim \frac{S}{V} \sim \frac{1}{r^2 \cdot r} = \frac{1}{r^3},$$

while the stress invariant scales as:

$$\sigma(r) \sim \frac{1}{r^3} \quad \text{for Schwarzschild.}$$

This suggests a correspondence between local entropy density and the magnitude of the stress invariant near gravitational collapse, though this is not a formal derivation. Similar ideas appear in holographic bounds on curvature from black hole thermodynamics [19]. Another route involves the observation that several quantum gravity proposals, including loop quantum gravity and causal set theory, posit that the Riemann tensor components or curvature invariants cannot exceed a maximal value [20,21]. In these models, there exists a maximum curvature scale $K_{\max}$ of order:

$$K_{\max} \sim \frac{1}{\ell_{\mathrm{QG}}^4},$$

where ℓ_{QG} is the fundamental length scale of the theory. If the failure threshold coincides with this limit, then:

$$\sigma_c \sim \frac{1}{\ell^4_{\mathrm{QG}}},$$

aligning with the phenomenological model adopted here. This again provides a dimensional scaffold rather than a unique derivation.

Each of these approaches remains speculative. No complete derivation of σ_c from first principles currently exists. However, the convergence of different lines of reasoning dimensional analysis, entropy scaling, and maximum curvature arguments supports the plausibility of treating σ_c as a fundamental cutoff parameter linked to the microstructure of spacetime. A rigorous derivation would require embedding the substrate stress framework into a specific quantum gravitational formalism. In future work, this direction could be pursued by examining how discrete structures in loop quantum gravity, causal sets, or string theory respond to increasing curvature. If the continuum limit of such a theory yields a stress field matching $\sigma(r,\theta)$ in the weak-field limit but breaks down at a consistent threshold, this would provide the desired derivation. Until then, the present framework provides a testable, covariant model in which classical geometry may fail in high-curvature regimes.

Having outlined the conceptual and quantum-geometric motivations for treating σ_c as a fundamental curvature threshold, it is natural to ask whether such a failure surface can produce observable consequences. In particular, if the region $r < r_c(\theta)$ behaves as a reflective or non-geometric interior, then gravitational waves interacting with this boundary may generate time-delayed echoes in the post-merger signal of rotating black hole binaries. The remainder of this section examines the observational implications of this possibility. The curvature-based failure surface defined by the condition $\sigma(r,\theta) = \sigma_c$ introduces several potential observational and conceptual implications. One such implication arises from the possibility that gravitational waves encountering the failure surface may reflect, giving rise to time-delayed echoes in the post-merger signal of black hole coalescence events.

To estimate the echo delay time, recall that the substrate model predicts the scalar curvature stress invariant scales as

$$\sigma(r) \sim \frac{M}{r^3}.$$

Equating $\sigma(r) \sim M/r^3$ to the critical threshold $\sigma_c \sim 1/\ell_P^2$ yields

$$r_c^3 \sim M\,\ell_P^2, \qquad \Rightarrow \quad r_c = \left(M\,\ell_P^2\right)^{1/3}.$$

WITHDRAWAL

© 2025 by the author(s). Distributed under a Creative Commons CC BY license.

Preprints.org (www.preprints.org) | NOT PEER-REVIEWED | Posted: 11 December 2025 doi:10.20944/preprints202512.1076.v1

Here M is understood to be expressed in geometric units, where $G = c = 1$. In conventional SI/CGS units the corresponding expression is

$$r_c = \left(\frac{GM}{c^2} \ell_P^2 \right)^{1/3},$$

which reduces to the form used above once geometric units are adopted. Because the echo delay depends only logarithmically on the ratio r_+/r_c, the numerical estimate below is insensitive to this conversion.

For a black hole of mass $M = 10M_\odot$ and Planck length $\ell_P \approx 1.616 \times 10^{-33}$ cm, the failure radius is approximately

$$r_c \approx \left(10 \cdot (1.616 \times 10^{-33})^2\right)^{1/3} \approx 6.5 \times 10^{-22} \text{ cm}.$$

Taking the outer Kerr horizon to be at $r_+ \sim 10^6$ cm, the round-trip delay time between the horizon and the failure surface is estimated as

$$\Delta t \sim M \cdot \ln\left(\frac{r_+}{r_c}\right) \approx M \cdot \ln\left(\frac{10^6}{6.5 \times 10^{-22}}\right) \approx M \cdot \ln(1.5 \times 10^{27}).$$

Using $\ln(10^{27}) \approx 62.1$, and the conversion factor $1M_\odot \approx 4.93 \times 10^{-6}$ s, the delay time is

$$\Delta t \sim 62 \cdot 4.93 \times 10^{-5} \text{ s} \approx 3.0 \text{ ms}.$$

This timescale lies within the observable band of current interferometers such as LIGO and Virgo. Unlike other exotic compact object (ECO) models that assume a spherically symmetric reflective surface [13,22,23], the failure surface in this framework is anisotropic, with $r_c(\theta)$ taking an oblate form in the Kerr geometry. As a result, different angular modes particularly those with large $|m|$ reflect from deeper radii and exhibit longer delays, while polar modes reflect earlier. This angular structure implies a measurable spin-dependent spread in the echo signal, providing a unique falsifiable signature of the failure surface model. Beyond observational consequences, the presence of a finite-curvature failure surface alters the conceptual structure of the interior. In classical general relativity, curvature diverges at $r = 0$ and geodesics terminate at the singularity. Here, the breakdown occurs at $\sigma = \sigma_c$, providing a finite-curvature surface at which the continuum approximation fails. The region beyond r_c lacks a well-defined metric and may correspond to a non-geometric or discrete regime. While no specific microphysical model is proposed, this construction reframes the endpoint of classical evolution as a physical information boundary, rather than a mathematical divergence [1,11]. Such a boundary may provide a new conceptual handle on the black hole information problem, though quantitative resolution requires further development.

For astrophysical Kerr black holes, the maximum attainable curvature along the spin axis remains many orders of magnitude below any reasonable value of the critical stress σ_c. Explicitly, the axial stress satisfies $\sigma_{\max}(\theta = 0) \sim 10^{11}\,\text{cm}^{-2}$ for stellar-mass and supermassive black holes, whereas a Planck-scale threshold corresponds to $\sigma_c \sim 10^{66}\,\text{cm}^{-2}$. Thus the condition $\sigma(r,\theta) = \sigma_c$ always admits a finite solution for every latitude, ensuring that the failure surface forms a fully closed oblate surface rather than an open equatorial shell. This removes any ambiguity regarding the global topology of the surface and guarantees that the continuum termination encloses the would-be ring singularity at all spins.

10. Conclusions

The analysis presented here extends the curvature-based substrate stress framework from the Schwarzschild solution to the Kerr geometry. Using the exact Kerr Kretschmann scalar, the local stress invariant $\sigma(r,\theta) = \sqrt{|K(r,\theta)|}$ was evaluated and used to determine the locus at which the continuum description reaches a critical stress threshold σ_c. The resulting failure surface $r_c(\theta)$ is intrinsically

WITHDRAWAL

© 2025 by the author(s). Distributed under a Creative Commons CC BY license.

Preprints.org (www.preprints.org) | NOT PEER-REVIEWED | Posted: 11 December 2025 doi:10.20944/preprints202512.1076.v1

anisotropic: it reaches its maximal radius in the equatorial plane, where curvature diverges most strongly, and its minimal radius along the rotation axis, where the stress remains finite even at $r = 0$. Within this framework, the classical ring singularity at $\Sigma = 0$ is never approached, as the curvature-stress threshold is encountered at a finite radius that functions as an internal geometric boundary. The structure obtained here reduces smoothly to the spherical failure radius derived in the Schwarzschild case, demonstrating that the substrate stress model behaves consistently across static and rotating spacetimes. The anisotropic surface $r_c(\theta)$ also shows that rotation modifies the internal curvature landscape independently of the horizon structure, since its location need not coincide with either Kerr horizon.

Several avenues for future investigation follow. A full numerical reconstruction of $r_c(\theta)$ across the parameter space (M, a, σ_c) would allow systematic comparison with other curvature scalars and with properties of geodesic motion. Extending the failure analysis to Kerr–Newman and Kerr–de Sitter geometries would test whether similar oblate structures arise in charged or cosmological settings. A more refined treatment of σ_c may be obtained by embedding the substrate model into quantum-gravity frameworks that posit upper bounds on curvature. Finally, the observational implications of anisotropic failure surfaces-including potential modifications to echo delays, mode-dependent reflection radii, and near-horizon propagation-justify dedicated time-domain simulations in nearly-Kerr backgrounds. Such signatures also provide a direct means by which future gravitational-wave observations could place empirical constraints on σ_c.

The results presented here indicate that the introduction of a finite curvature-stress threshold yields a coherent and covariant mechanism by which classical singularity formation in rotating collapse may be avoided. Further development of this framework may offer new insight into the internal structure of astrophysical black holes and the onset of non-classical geometric behavior at extreme curvature.

WITHDRAWAL

Author Contributions: This article is the sole work of the author.

Funding: No external funding was received for this work.

Institutional Review Board Statement: Not applicable.

Data Availability Statement: No datasets were generated or analyzed in this study.

Conflicts of Interest: The author declares no conflicts of interest.

References

1. Cody, M. (2025). *Black Hole Singularities and the Limits of the Spacetime Continuum*. Preprint.org.
2. Chandrasekhar, S. (1983). *The Mathematical Theory of Black Holes*. Oxford University Press.
3. Henry, R. C. (2000). *Kretschmann Scalar for a Kerr-Newman Black Hole*. The Astrophysical Journal, 535(1), 350–353.
4. Carroll, S. M. (2004). *Spacetime and Geometry: An Introduction to General Relativity*. Addison-Wesley.
5. Poisson, E. (2004). *A Relativist's Toolkit: The Mathematics of Black-Hole Mechanics*. Cambridge University Press.
6. Wald, R. M. (1984). *General Relativity*. University of Chicago Press.
7. Cherubini, C., Bini, D., Capozziello, S., & Ruffini, R. (2002). *Second Order Scalar Invariants of the Riemann Tensor: Applications to Black Hole Spacetimes*. International Journal of Modern Physics D, 11, 827–841.
8. Tenev, T., & Horstemeyer, M. F. (2018). *The elastic nature of spacetime*. International Journal of Modern Physics D, 27(12), 1850114.
9. Bini, D., Cherubini, C., Jantzen, R. T., & Ruffini, R. (2002). *Massless fields and scalar invariants of the Riemann tensor*. Progress of Theoretical Physics, 107(5), 967–992.
10. Page, D. N. (2006). *Kerr–de Sitter black holes with scalar curvature invariants*. Classical and Quantum Gravity, 23(18), 6239–6252.
11. Bardeen, J. M., Press, W. H., & Teukolsky, S. A. (1972). *Rotating black holes: Locally nonrotating frames, energy extraction, and scalar synchrotron radiation*. The Astrophysical Journal, 178, 347–370.
12. Barceló, C., Liberati, S., Sonego, S., & Visser, M. (2011). *Fate of gravitational collapse in semiclassical gravity*. Physical Review D, 83(4), 041501.

© 2025 by the author(s). Distributed under a Creative Commons CC BY license.

Preprints.org (www.preprints.org) | NOT PEER-REVIEWED | Posted: 11 December 2025 doi:10.20944/preprints202512.1076.v1

13. Cardoso, V., Franzin, E., & Pani, P. (2019). *Black holes and fundamental fields: Hair, echoes and shadows*. Living Reviews in Relativity, 22(1), 4.
14. Komissarov, S. S., Barkov, M. V., Vlahakis, N., & Königl, A. (2007). *Magnetic acceleration of ultrarelativistic jets in gamma-ray burst sources*. Monthly Notices of the Royal Astronomical Society, 380(1), 51–70.
15. Mathur, S. D. (2005). *The fuzzball proposal for black holes: An elementary review*. Fortschritte der Physik, 53(7), 793–827.
16. Mazur, P. O., & Mottola, E. (2004). *Gravitational vacuum condensate stars*. Proceedings of the National Academy of Sciences, 101(26), 9545–9550.
17. Ashtekar, A., Pawlowski, T., & Singh, P. (2006). *Quantum Nature of the Big Bang: Improved Dynamics*. Physical Review D, 74(8), 084003.
18. Modesto, L. (2006). *Loop quantum black hole*. Classical and Quantum Gravity, 23(18), 5587–5602.
19. Bousso, R. (2000). *The holographic principle*. Reviews of Modern Physics, 74(3), 825–874.
20. Hossenfelder, S. (2013). *Minimal Length Scale Scenarios for Quantum Gravity*. Living Reviews in Relativity, 16(2).
21. Rovelli, C., & Vidotto, F. (2015). *Covariant Loop Quantum Gravity*. Cambridge University Press.
22. Abedi, J., Dykaar, H., & Afshordi, N. (2017). *Echoes from the abyss: Evidence for Planck-scale structure at black hole horizons*. Physical Review D, 96(8), 082004.
23. Cardoso, V., Hopper, S., Macedo, C. F. B., Palenzuela, C., & Pani, P. (2016). *Gravitational-wave signatures of exotic compact objects and of quantum corrections at the horizon scale*. Physical Review D, 94(8), 084031.

Disclaimer/Publisher's Note: The statements, opinions and data contained in all publications are solely those of the individual author(s) and contributor(s) and not of MDPI and/or the editor(s). MDPI and/or the editor(s) disclaim responsibility for any injury to people or property resulting from any ideas, methods, instructions or products referred to in the content.

WITHDRAWAL

© 2025 by the author(s). Distributed under a Creative Commons CC BY license.